ISSN (Print) 1226-1750
ISSN (Online) 2233-6656
Journal of Magnetics 25(4), 587-594 (2020) https://doi.org/10.4283/JMAG.2020.25.4.587

The Applications of Radiomics for Predicting Survival Rate of Patients with Head and Neck Squamous Cell Carcinoma (HNSCC)

Sang Won Park[1,2], Payam Hosseinzadeh Kasani[2], Na Young Yeo[3], Gab-Jung Kim[4], Se-Jong Yoo[5], and Jin Su Kim[6,7]*

[1]*Department of Medical Bigdata Convergence, Kangwon National University, Chuncheon 24341, Republic of Korea*
[2]*Department of Neurology, Kangwon National University Hospital, Chuncheon 24289, Republic of Korea*
[3]*Department of Advanced Research and Development, Hanhwa Hightech Corp., Daejeon 34129, Republic of Korea*
[4]*Department of Radiological Technology, Songho University, Hoengseong 25242, Republic of Korea*
[5]*Department of Radiological Technology, Daejeon Health Institute of Technology, Daejeon 34504, Republic of Korea*
[6]*Radiologcial and Medico-Oncological Sciences, University of Science and Technology (UST) Seoul 01812, Republic of Korea*
[7]*Division of RI Application, Korea Institute Radiological and Medical Sciences, Seoul 01812, Republic of Korea*

(Received 26 October 2020, Received in final form 20 November 2020, Accepted 20 November 2020)

The radiomics based on positron emission tomography (PET) data and random forest can predict overall survival rate of head and neck squamous cell carcinoma (HNSCC). We used the texture features extracted from PET and clinical information from patients with HNSCC (n = 138). The Spearman's correlation analysis, Kaplan-Meier log rank test and random forest were used for survival significance and to predict survival rate of patients with HNSCC. Zone Length Non-Uniformity (ZLNU) was defined as a new key radiomics feature to predict survival rate. For stage N2 group, predicted survival rate was 76.2 % and actual survival rate was 73.3 %. For stage IVA group, predicted survival rate was 74.7 % and actual survival rate was 73.8 %. The result of this study that applications of ^{18}F-(FDG)-PET images using radiomics features was validated and could be expected to be used as the basis for future research using MRI images with more distinct structures.

Keywords : HNSCC, radiomics, survival analysis, positron emission tomography, medical image analysis, MRI application

1. Introduction

Head and neck squamous cell carcinomas (HNSCC) is known as the sixth most common malignant tumors in the world more than twice lung cancer and cervical cancer [1]. HNSCC is a type of cancer and mainly manifests in regions of pharynx and the larynx with the exception of the eyeball, brain, ears, and esophagus. Specifically, there could be shown the region including such as the frontal sinus, nasal cavity, oral cavity, tongue, and salivary glands at least 30 [2]. HNSCC usually appear as a type of squamous cells and the main causes of this disease are known smoking, drinking, and human papillomavirus (HPV) infection. In addition, the survival rate in patients is correlated with lymph node status and the degree of cancer metastasis [3-5]. More than 60 % of patients with HNSCC could have a death within five years. However, if they were treated in early, the survival rate could be up to 90 % [6]. Despite the levels of high risk and rapid increment of HNSCC, awareness for the seriousness of this disease remains low [3].

HNSCC histopathological grades could be evaluated by biopsy, surgical resection and medical image such as magnetic resonance image (MRI) and computed tomography (CT) quantitative analysis [7-9]. The quantitative assessment using medical images could provide for the prediction of clinical results such as survival rate and prognosis of tumor in patients based on MR or CT data [10, 11]. MRI was used to predict survival rate for the hepatocellular carcinoma, non-small cell lung cancer, and rectal carcinoma and CT scan was performed to make a decision for the Epidermal Growth Factor Receptor (EGFR) identifier [12-15]. ^{11}C-methionine (MET) positron emission tomography (PET) with anatomical structure based on MRI image radiomics also were conducted for distin-

*Corresponding author: Tel: +82-2-970-1662
Fax: +82-2-970-2416, e-mail: kjs@kirams.re.kr

guishing recurrent brain tumor from radiation necrosis based [16].

One of the quantitative analysis tool is known the radiomics through extracting features from medical images. It could be used to predict prognosis through correlation with clinical information and statistical such as random forest [11, 16]. Random forests were an ensemble learning method for classification, regression, and prediction. Random forest was widely used for survival prediction for space extensions for censored data, for drug sensitivity prediction, for prediction forest change, for prediction of spatial distribution of sediment pollution in an estuarine system [17-20].

In this study, we focus on the radiomics using PET data for prediction survival rate through random forest and assess the validation by comparing results of patient's actual survival rate with prediction results.

2. Experimental Methods

2.1. Subjects data

The data of subjects in this study were acquired from the The Cancer Imaging Archive (TCIA) database (https://www.cancerimagingarchive.net/collections/) and downloaded on November 20, 2018. We were approved for this study by institutional review board of Kangwon National University (KNUH-2020-07-006) and did not have any access to identify for the participated patients. We used only de-identified data approved by the institutional review board (https://cancerimagingarchive.net). The data including images and clinical information for the total of 138 patients who were diagnosed with HNSCC over up to 10-year follow-up period from 2006 to 2016 and whether alive or dead after radiation therapy, chemotherapy, and surgical operation. All patients were classified into TNM staging (Table 1), since the characteristics of patients with HNSCC such as distribution to multiple metastasis or progression state. Moreover, the patient's data were used to determine main factors through correlation analysis between features extracted from PET data and clinical information.

Table 1. Demographic data of HNSCC patients.

Patient characteristic	Study population (n = 138)
Cause of death	
Alive	95 (69 %)
HN cancer	27 (20 %)
Other cancer	6 (4 %)
Non cancer related	4 (3 %)
Unknown	6 (4 %)
T stage	
T1–T2	66 (48 %)
T3–T4	72 (52 %)
N stage	
N0–N1	25 (18 %)
N2–N3	113 (82 %)
Overall stage	
I-II	3 (2 %)
III-IV	135 (98 %)
Site of diagnosis	
[1]Oral cavity	106 (77 %)
[2]Pharynx	11 (8 %)
Larynx	3 (2 %)
[3]etc.	18 (13 %)
Histopathology grade	
G1	11 (8 %)
G2	63 (46 %)
G3	64 (46 %)
Location of primary cancer	
Glottis	14 (10 %)
[4]Pharynx	124 (90 %)

[1]BOT = 54, Retromolar trigone = 1, Soft palate = 3, Tonsil = 48, [2]Glossopharyngeal sulcus = 1, hypopharynx = 2, oropharynx = 1, pharyngeal = 1, posterior pharyngeal wall = 1, NPC = 5, [3]supraglottic = 11, pyriform sinus = 7, [4]Pharynx includes the oropharynx, nasopharynx, and hypopharynx

2.2. PET

Data were collected using GE Medical Systems Discovery RX, Discovery ST and Discovery STE hybrid

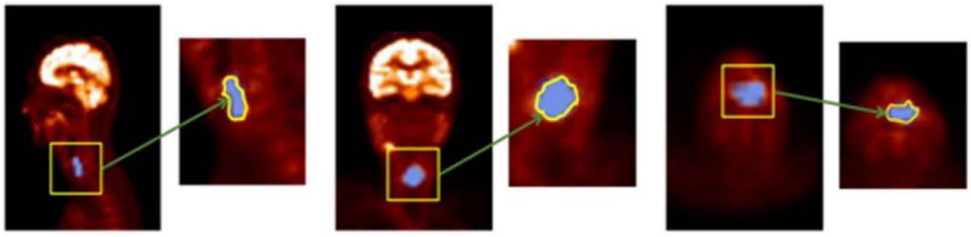

Fig. 1. (Color online) ROI delineation for radiomics. ROIs were drawn by PET image specialist. All regions such as glottis, hypopharynx, nasopharynx were included for ROT delineation. The tumor size was ranged from 2.04 cm^3 to 89.72 cm^3, and a mean size was 26.09 cm^3. The LIFEx (www.lifexsoft.org, Orsay, France) program was used for radiomics feature extraction. A total of 26 texture features were extracted.

PET/CT scanner. The PET scan was performed for 30 minutes after 20 minutes ^{18}F-FDG intravenous(IV) administration [21]. All processes for the patients conducted scan comply with the guidelines of European Association of Nuclear Medicine (EANM) [22]. All images were processed attenuation correction to minimize the artifact or scatters and performed the normalization to make standardized images for analysis. Voxel size in reconstruction of PET data was $4 \times 4 \times 4$ cm^3 and intensity was rescaled to 64 grey levels.

2.3. Features extraction and Tumor selection

Many features extracted from medical images could not be correlated with the outcome or might show the correlation with other disease in standard clinical by causing chaos through radiomics. After perform the feature extraction, the selection of the number of features to reduce is the necessary step in all process of radiomics [23]. However, the remaining features also could not give the informative source since the range of features are in the hundreds [24].

Thus, the overfitting risk is not trivial and some external validations could be required to fit the proper model performance [25]. The main method for extracting features from medical imagaes is to select region of interest (ROI) on the disease lesion in images. We had been conducted selection ROI on the region of disease of PET (Fig. 1). ROI contours were defined by a qualified professional (e.g., radiation oncologist) and investigated semi-automatically by PET image specialist. Some differences could occur between observers and software, that could make a result in a significant difference in feature values. Thus, we have been conducted addressed partially by intra-observing variability of ROI and reduce significant error across observers. All regions such as glottis, hypopharynx and nasopharynx were included for ROI delineation (Fig. 1).

The total of tumor size was ranged from 2.04 cm^3 to 89.72 cm^3, and a mean size was 26.09 cm^3. We used the LIFEx (www.lifexsoft.org, Orsay, France) for feature extraction process and total of 26 texture features were extracted. Table 2 shows texture feature used in this study [26].

2.4. Statistical analysis - Spearman's correlation, Kaplan-Meier log-rank test, and random forest analysis

The radiomics features that could be used and related to analyze and predict for survival rate were selected by performing Spearman's correlation analysis between texture features and clinical information from patients classified by TNM staging. As for the designation of survival time of the patients, the time of the last visit was the reference point for correlation analysis for surviving patients (censored) and date of death was the reference point for survival analysis for the patients who died (uncensored). However, for dead patients who survived longer than or equal to the last visit time of surviving patients, the average survival time of the surviving patients was used

Table 2. HNSCC patients based on TNM and tumor progression.

Groups (n=138)	Male	Female	Age	
			(mean ± SD)	Median (IQR*)
HNSCC subtype				
SCC (n=138)	113	25	57.54 ± 10.16	57.00 (50.25 ± 64.00)
T stage				
T1 (n=21)	20	1	55.14 ± 10.73	58.00 (47.00 ± 63.00)
T2 (n=45)	35	10	56.91 ± 10.05	55.00 (51.00 ± 62.00)
T3 (n=41)	35	6	59.48 ± 7.61	59.00 (53.00 ± 64.00)
T4 (n=31)	23	8	57.48 ± 12.19	58.00 (48.00 ± 67.00)
N stage				
N0 (n=13)	7	6	58.53 ± 8.40	58.00 (53.00 ± 64.00)
N1 (n=12)	11	1	57.91 ± 6.14	58.00 (53.25 ± 63.50)
N2 (n=101)	84	17	57.71 ± 10.48	56.00 (50.00 ± 65.00)
N3 (n=12)	11	1	54.58 ± 11.70	59.50 (44.50 ± 61.50)
Overall stage				
II (n=3)	1	2	56.67 ± 3.77	54.00 (54.00 ± 58.00)
III (n=18)	16	2	58.5 ± 8.25	59.00 (51.50 ± 64.75)
IVA (n=103)	83	20	57.63 ± 10.10	56.00 (51.00 ± 64.50)
IVB (n=14)	13	1	55.79 ± 13.13	59.50 (45.00 ± 62.50)

*Inter Quartile Range

[27]. In order to extract the exact factors that are less affected by multiple variables among the posterior prediction factors observed through correlation analysis, Holm-Bonferroni correction was performed ($p < 0.05$). The distribution of event time (days from first diagnosis to death or last visit) required for application of the Kaplan-Meier log-rank test was calculated. The results obtained were converted to $-\log_{10}{}^{p}$ values and Holm-Bonferroni correction was applied. The results of Spearman correlation analysis and Kaplan-Meier log-rank test were expressed using a heat-map to show the correlations between clinical information and texture features.

Lastly, random forest analysis was performed using the common factors selected from the above two analyses. Spearman correlation analysis and Kaplan-Meier log-rank test were performed with SPSS (v 21.0). Holm-Bonferroni correction and random forest analysis were performed using R (v 3.6.1).

Table 3. Radiomics features.

HISTO	Skewness, Kurtosis, Energy
GLCM	Homogeneity, Contrast, Correlation, Dissimilarity
GLRLM	SRE, LRE, LGRE, HGRE, GLNU, RLNU
NGLDM	Coarseness, Contrast, Busyness
GLZLM	SZE, LZE, LGZE, HGZE, SZLGE, SZHGE, GLNU, ZLNU, ZP

HISTO : histogram; GLCM : Gray Level Co-occurrence Matrix; GLRLM : The Grey-Level Run Length Matrix; SRE : Short-Run Emphasis; LRE : Long-Run Emphasis; LGRE : Low Gray-level Run Emphasis; HGRE : High Gray-level Run Emphasis; GLNU : Gray-Level Non-Uniformity; RLNU : Run Length Non-Uniformity; NGLDM : The Neighborhood Grey-Level Different Matrix; GLZLM : The Grey-Level Zone Length Matrix; SZE : Short-Zone Emphasis; LZE : Long-Zone Emphasis; LGZE : Low Gray-level Zone Emphasis; HGZE : High Gray-level Zone Emphasis; SZLGE : Short-Zone Low Gray-level Emphasis; SZHGE : Short-Zone High Gray-level Emphasis; GLNU : Gray-Level Non-Uniformity; ZLNU : Zone Length Non-Uniformity; ZP : Zone Percentage

3. Results and Discussion

3.1. Patient characteristics

A total of 138 patients were included in this study for analysis (Table 3). The tumor type in all patients was HNSCC, and the subjects included 113 males (82 %) and 25 females (18 %). The mean patient age was 57.54 ± 10.16 years, and the average size of the tumor was 26 cm^3. Eighty-four patients (61 %) were smokers, while 54 were non-smokers (39 %). Patients underwent treatment methods included concurrent chemo-radiotherapy (CCRT) in 44 patients (32 %), external radiation therapy (ERT) in 19 patients (14 %), and ERT + surgery in 9 patients (7 %). Diagnosis and patient prognosis after treatment showed survival in 95 patients (69 %) and death in 43 patients (31 %). The causes of death included direct effects of HNSCC in 27 patients (20 %), cancer metastasis to other organs and tissues in 6 patients (4 %), causes unrelated to cancer in 4 patients (3 %), and unknown causes in 6 patients (4 %). When patients were categorized according to disease progression, T1-2 included 66 patients (48 %), T3-4

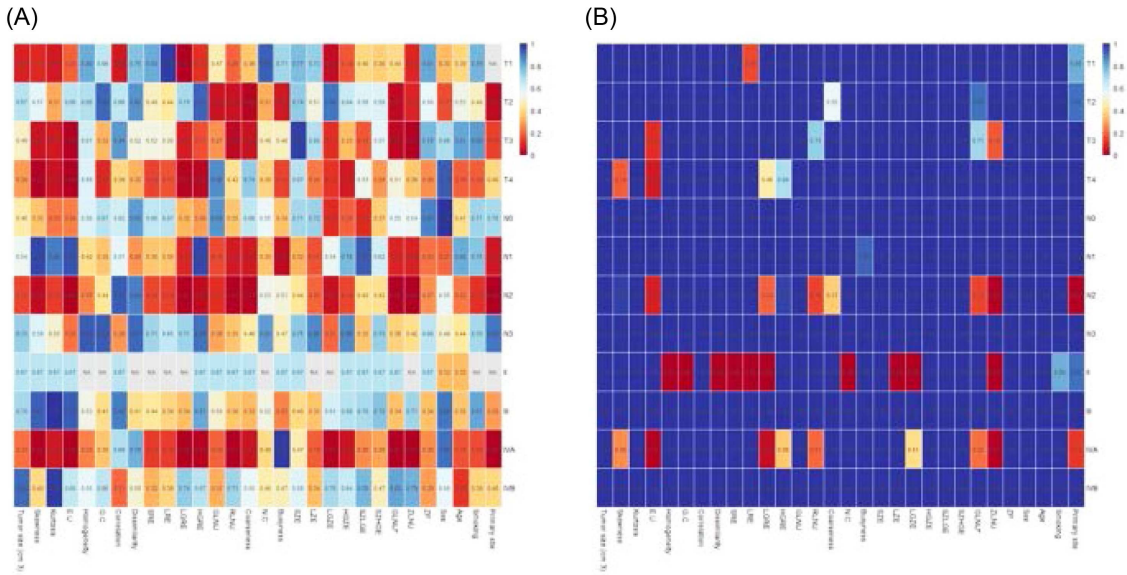

Fig. 2. (Color online) Heat-map of Spearman's correlation analysis between clinical data and radiomics features (A) without Holm-bonferroni correction, (B) with Holm-bonferroni correction. After Holm-Bonferroni correction, radiomics features such as ZLNU for group N2 and 3 radiomics features such as Energy Uniformity, LGRE, ZLNU for IVA were correlated with primary site in clinical information. ZLNU was common radiomics feature for both stage N2 and stage IVA groups.

included 72 patients (52%), N0-1 included 25 patients (18 %) and N2-3 included 113 patients (82 %). In addition, 3 patients (2 %) showed stage I-II overall tumor progression, while 135 patients (98 %) showed stage III-IV overall tumor progression, indicating that the number of patients with advanced tumor progression was higher. The location of the primary tumor at initial diagnosis was the pharynx in 124 patients (90 %) and the glottis in 14 patients (10 %).

3.2. Spearman's correlation analysis

Spearman's correlation analysis provided the correlation between clinical information and radiomics features to select a few significant radiomics features that were related to the patients' survival in the T, N, and stage groups (Fig. 2).

Heat map of spearman correlation between stage and radiomics features was shown in Fig. 2A. In T, N2, IVA group, 9 radiomics features such as Skewness, Energy Uniformity, Low Gray-level Run Emphasis (LGRE), High Gray-level Run Emphasis (HGRE), Run Length Non-Uniformity (RLNU), Low Gray-level Zone Emphasis (LGZE), Gray-Level Non-Uniformity (GLNU), Zone Length Non-Uniformity (ZLNU) were highly correlated with clinical information ($p < 0.05$). For T4 group, 5 radiomics features such as Skewness, Kurtosis, Energy Uniformity, LGRE, HGRE were found. For the N groups, 1 feature (Busyness) for NI and 10 features (such Skewness, Energy Uniformity, LGRE, HGRE, RLNU, Coarseness, LGZE, GLNU, ZLNU, Primary site) for N2 were correlated with clinical data ($P < 0.05$). N2 and IVA groups showed high correlation with clinical data and survival significance when Spearman correlation analysis was performed. The Spearman's correlation coefficient ranged 0.001 to 0.048.

For IVA group, 8 radiomics features such as Skewness, Energy Uniformity, LGRE, HGRE, RLNU, LGZE, GLNU, ZLNU were correlated with clinical information. After Holm-Bonferroni correction, radiomics features such as ZLNU for group N2 and 3 radiomics features such as Energy Uniformity, LGRE, ZLNU for IVA were correlated with clinical information (Fig. 2B). Finally, ZLNU was common radiomics feature for both stage N2 and stage IVA groups.

3.3. Kaplan-Meier log rank test

Kaplan-Meier log rank test provided radiomics features that showed survival significance ($p < 0.05$). Kaplan-Meier log rank test was performed All groups, with the exception of the stage II group, exhibited texture features that indicated significance of survival (Fig. 3A). The 4 features (such as skewness, HGRE, HGZE, primary site) were common factor across the T, N, and stage groups. For T4 group, six radiomics features such as skewness, energy uniformity, LGRE, HGRE, SZE, HGZE were found. For N2 group, 2 radiomics features such as kurtosis and coarseness were found. For IVA group, 5 radiomics features such as skewness, kurtosis, HGRE, coarseness, HGZE were found (Fig. 3B).

3.4. Random Forest analysis

As a result of the analysis for the Spearman's corre-

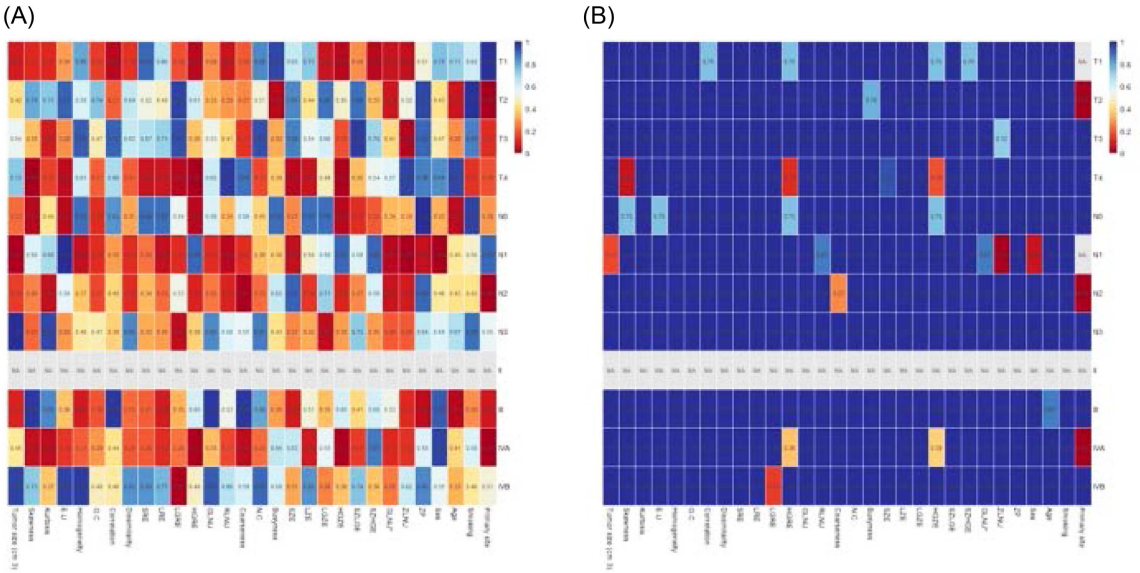

Fig. 3. (Color online) Heat-map of Kaplan-Meier log rank test (A) without Holm-bonferroni correction, (B) with Holm-bonferroni correction. After Holm-Bonferroni correction, ZLNU was selected as radiomics feature of key factor to predict survival rate.

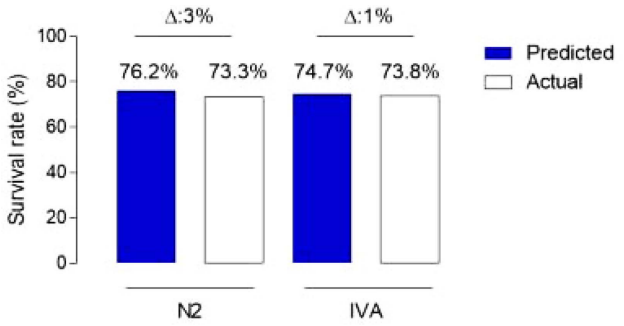

Fig. 4. (Color online) Survival rate prediction using Random Forest and ^{18}F-FDG PET based radiomics For N2 group, predicted survival rate was 76.2 % and actual survival rate was 73.3 %. For IVA group, predicted survival rate was 74.7 % and actual survival rate was 73.8 %. The difference between groups were 3 % for N2 group and 1% for IVA group.

lation and Kaplan-Meier, we could regard to N2 and IVA groups, which appear in common, as target groups to perform Random Forest. ZLNU, which shows a significant correlation between group and texture features in both N2 and IVA groups, was selected as the main factor to conduct Random Forest. Although the ZLNU feature does not show due to slight difference as the Holm-Bonferroni correction result of the Kaplan-Meier result, it has significance correlation coefficient in both N2 and IVA groups. Figure 4 shows the survival rate prediction using random forest analysis. For N2 group, predicted survival rate was 76.2 % and actual survival rate was 73.3 %. For IVA group, predicted survival rate was 74.7 % and actual survival rate was 73.8 %. The difference between groups were 3 % for N2 group and 1 % for IVA group. Cumulative survival rates and survival curve for calculating the

Table 4. Demographic data of HNSCC patients based on clinical data.

Patient characteristic	Study population (n = 138)
Sex	
Male	113 (82 %)
Female	25 (18 %)
Age (years, mean ± SD)	57.54 ± 10.16
[1]Smoking	
Yes	84 (61 %)
No	54 (39 %)
[2]Treatment	
C.C	44 (32 %)
C.C+C	18 (13 %)
C.C+S	19 (14 %)
C+C.C+S	7 (4 %)
C+E	16 (12 %)
C+E+S	6 (4 %)
E	19 (14 %)
E+S	9 (7 %)
Death	
Yes	43 (31 %)
No	95 (69 %)

[1]Patients were defined as "ever smokers" if they smoked at least 100 cigarettes during their lifetime, and "never smokers" otherwise.
[2]HNSCC patients can be treated in a variety of ways, depending on the stage, severity, and metastasis. Eight types of treatment were performed for patients in this study. The definitions of the abbreviations are as follows.
C.C : Concurrent Chemo-radiotherapy, C : Chemotherapy, E : External beam radiotherapy, S : Surgery

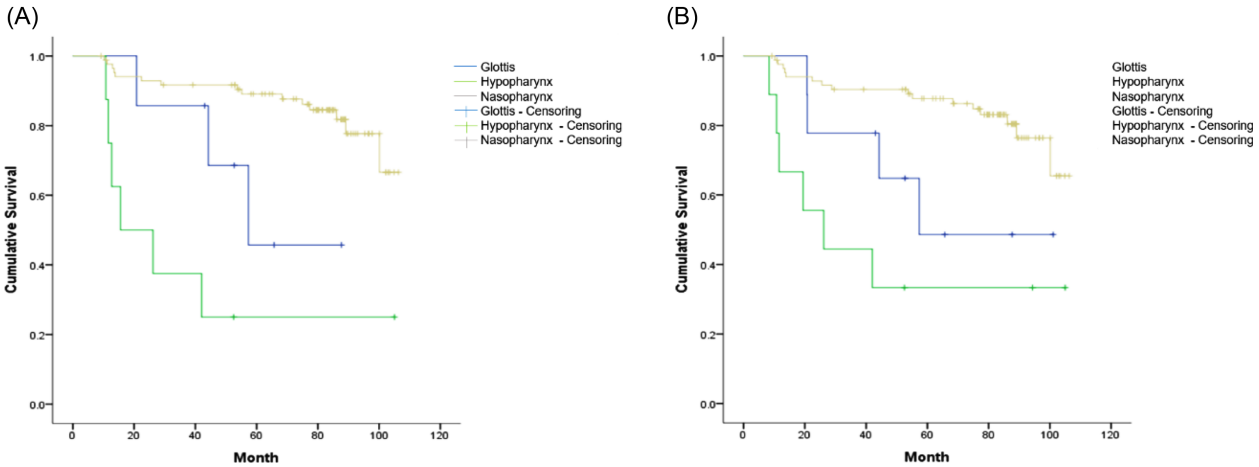

Fig. 5. (Color online) Survival curve for prediction survival rate using random forest through ^{18}F-FDG PET based radiomics in N2 and IVA group. (A) The survival rates of Glottis, Hypopharynx, and Nasopharynx Glottis using texture features (Primary site) of patients in N2 group were 42.85 %, 75 %, and 17.44 %, respectively and survival time (mean ± SD) was 63.74 ± 10.10, 41.09 ± 13.48, 94.03 ± 3.00 months. (B) The survival rates of Glottis, Hypopharynx, and Nasopharynx Glottis using texture features (Primary site) of patients in IVA group were 44.40 %, 66.70 %, and 18.80 %, respectively and survival time (mean ± SD) was 68.77 ± 11.85, 48.13 ± 13.77, 92.96 ± 3.13 months.

value of actual survival rate in representative site of N2 and IVA are presented in the Figure 5 (Table 4).

3.5. Discussion

We conducted to predict the survival rate of patients with HNSCC and compare with actual survival rate based on the FDG PET through radiomics. The result of comparison between prediction and actual survival rate get almost no difference, as a novelty in this study. To perform the radiomics quantitative analysis using texture features, statistical method was investigated. Random forest is one of the statistical method known to be one of the effective and classification algorithms that runs efficiently on large databases with thousands of input variables [28]. As the paradigm of medical care has recently changed, the demand for diagnosis and treatment plans has increased based on objective and quantitative information rather than subjectivity based on experience [29]. Accordingly, it is required to improve the value of the quantitative image biomarker, in this reason we conducted our study using random forest for appropriate prediction of survival prediction.

The HNSCC stage was classified on the basis of the TNM system, which may indicate the overall stage of disease progression. Although there are slight differences depending on the affected regions (oral cavity, pharynx, larynx, etc.), the T parameters classified into TX, wherein the primary tumor cannot be assessed, through T1, where the maximum size of the tumor is 2 cm or below, and up to T4b, where the base of the skull is invaded or the internal carotid artery is surrounded. The N parameters divided into categories ranging from NX, wherein the local lymph tumor cannot be assessed, up to N3, where a lymphoma of at least 6 cm in size is in metastasis. In addition, the cases can be further classified using grades MX–M1 according to the degree of metastasis (30). Patient included in this study was divided into 12 groups depending on T (T1-T4), N (N1-N4), stage (II-IVB), feature extracted from the clinical information (age, gender, survival, location of primary tumor, smoking, etc.), and PET data. Analysis was conducted for the divided HNSCC patients into 12 groups depending on T (T1-T4), N (N1-N4) and stage (II-IVB), and the feature values extracted from the PET images and clinical information (age, gender, survival, location of primary tumor, smoking, etc.) in each group.

The following three statistical analyses were conducted in order to extract significant texture features that could be used in survival analysis and survival prediction measurement in patients. First, Spearman's correlation analysis was used to analyze the correlation between clinical information and texture features in order to select a few significant texture features that were related to the patients' survival in the T, N, and stage groups. 70-80 % of HNSCC diagnoses was associated with tobacco and alcohol use [31]. However, in this study, tobacco use was not significant factor during Spearman's correlation analysis. The only significant factor in clinical information was the region of primary site. Subsequently, Kaplan-Meier log rank test was used to select the radiomics features that showed survival significance. Lastly, random forest analysis was used to predict survival rate in patients with HNSCC. The results of predicted survival rate using random forest and radiomics were nearly identical. The differences between groups were < 3 % for N2 and < 1 % for IVA groups, respectively. According to the systematic review HNSCC from Creff *et al.*, The FDG-PET/CT volumetric parameters (metabolic tumor volume [MTV] and total lesion glycolysis [TLG]) were independent prognostic factors in most of the data, with a higher prognostic value than the maximum standard uptake value SUV_{max} [32]. For example, in univariate analysis of OS, the SUV_{max} was correlated with OS in 5 of 11 studies, MTV in 11 of 12 studies, and TLG in 6 of 9 studies [32].

In this study, we performed random forest to predict survival rate of HNSCC. Among the multiple parameters of radiomics, ZLNU was selected as a key radiomics feature to predict survival rate in patients with HNSCC after Holm-Bonferroni correction, Spearman's correlation, and Kaplan-Meier log rank test. ZLNU was also found important radiomics feature for evaluation of CT based radiomics in patients with laryngeal squamous cell carcinoma [33], for FDG PET based radiomics in patients with breast cancers [34], for CT based radiomics in patients with squamous cell carcinoma from adenocarcinoma [35], for contrast enhanced MR based radiomics in patients with sentinel lymph node metastasis in breast cancer [36], for CT based radiomics in patients with HNSCC [37].

Limitation of this study was that the number of patients in the 12 groups was different, which may affect the significance of Spearman's correlation analysis and Kaplan-Meier log rank test. In addition, when calculating the survival periods of the patients, the date of death was the last visit time for the surviving patients (censored) or the baseline in the correlation analysis for the dead patients (uncensored), and the mean survival period was assigned for dead patients whose actual survival period was the same or longer than the last visit time of the surviving patients [27].

4. Conclusion

In conclusion, we showed that preoperative survival rate prediction could be implemented using ^{18}F-FDG PET based radiomics and random forest in patients with HNSCC. Random forest and FDG PET based radiomics could be used for preoperative survival rate prediction in patients with HNSCC. In addition, this present results could be expected to be used as the basis for future research using MRI images with more distinct structures.

Acknowledgement

This study was funded by Ministry of Science and ICT (MSIT), Republic of Korea. (NRF-2020R1F1A1061476, 50536-2020, 50461-2019).

References

[1] Y. S. Lee, J. Koran Otorhinolaryngology-Head and Neck Surgery **62**, 9 (2019).
[2] X. Qian, B. Sinikovic, F. Schreiber, S. Ochsenreither, K. Klinghammer, B. Wollenberg, A. M. Kaufmann, and A. E. Albers, Eur. Arch. Otorhino-laryngol. **275**, 11 (2018).
[3] M. Hotta, R. Minamimoto, and K. Miwa, Sci. Rep. **9**, 1 (2019).
[4] N. Subramaniam, S. Murthy, D. Balasubramanian, T. H. Low, S. Vidhyadharan, J. R. Clark, K. Thankappan, and S. Iyer, Head & Neck **40**, 10 (2018).
[5] Q. S. Xu, C. Wang, B. Li, J. Li, M. H. Mao, L. Z. Qin, H. Li, X. Huang, Z. Han, and Z. Feng, J. Oral. Dis. **24**, 3 (2018).
[6] F. Janot, J. Klijanienko, A. Russo, J. Mamet, F. De Braud, A. K. El-Naggar, J. P. Pignon, B. Luboinski, and E. Cvitkovic, Br J. Cancer. **73**, 4 (1996).
[7] W. Wu, J. Ye, Q. Wang, J. Luo, and S. Xu, Front Oncol. **9**, (2019).
[8] C. Bourgier, J. Colinge, N. Ailleres, P. Fenoglietto, M. Brengues, A. Pelegrin, et al., Cancer Radiother. **19**, 6 (2015).
[9] P. Lambin, E. Rios-Velazquez, R. Leijenaar, S. Carvalho, R. G. Van Stiphout, P. Granton, C. M. L. Zegers, R. Gillies, R. Boellard, A. Dekker, and H. J. W. L. Aerts, Eur J. Cancer. **48**, 4 (2012).
[10] X. Li and H. Zhao, Stat. Interface **2**, 2 (2009).
[11] H. Zhang, C. M. Graham, O. Elci, and M. E. Khan, J. Radiol. **269**, 3 (2013).
[12] B. He, T. Ji, H. Zhang, Y. Zhu, R. Shu, W. Zhao, and K. Wang, J. Cell Physiol. **234**, 11 (2019).
[13] T. P. Coroller, V. Agrawal, E. Huynh, V. Narayan, S. W. Lee, and R. H. Mak, J. Thorac. Oncol. **12**, 3 (2017).
[14] A. J. Grossberg, A. S. Mohamed, H. Halawani, W. C. Bennett, K. E. Smith, T. S. Nolan, Bowman Williams, S. Chamchod, J. Heukelom, M. E. Kantor, T. Browne, K. A. Hutcheson, G. BrandonGunn, A. S. Garden, W. H. Morrison, S. J. Frank, D. I. Rosenthal, J. B. Freymann, and C. D. Fuller, Sci. Data. **5**, (2018).
[15] W. H. Wang, L. H. Long, Y. Cui, A. Y. Jia, X. G. Zhu, and H. Z. Wang, Br J. Cancer. **122**, 7 (2020).
[16] A. Fujita, K. Buch, B. Li, Y. Kawashima, M. M. Qureshi, and O. Sakai, J. Comput. Tomogr. **40**, 1 (2016).
[17] H. Wang and L. Zhou, Artif. Intell. Med. 79, (2017).
[18] R. Rahman, K. Matlock, S. Ghosh, and R. Pal, Sci. Rep. **7**, 1 (2017).
[19] F. Santos, V. Graw, and S. Bonilla, PLoS ONE **14**, 12 (2019).
[20] E. S. Walsh, B. J. Kreakie, M. G. Cantwell, and D. Nacci, PLoS ONE **12**, 7 (2017).
[21] I. Castiglioni, F. Gallivanone, P. Soda, M. Avanzo, J. Stancanello, and M. Aiello, EJNMMI **1**, (2019).
[22] R. Boellaard, R. Delgado-Bolton, W. J. Oyen, F. Giammarile, K. Tatsch, and W. Eschner, EJNMMI **42**, 2 (2015).
[23] A. Ibrahim, M. Vallieres, H. Woodruff, S. Primakov, M. Beheshti, S. Keek, et al., editors. Semin Nucl. Med. (2019).
[24] D. M. Hawkins, J. Chem. Inform. Comput. Sci. **44**, 1 (2004).
[25] P. Lambin, R. T. Leijenaar, T. M. Deist, J. Peerlings, E. E. C. De Jong, and J. V. Timmeren, Nat. Rev. Clin. Oncol. **14**, 12 (2017).
[26] C. Nioche, F. Orlhac, S. Boughdad, S. Reuze, J. Goya-Outi, C. Robert, et al., Cancer Res. **78**, 16 (2018).
[27] A. Chaddad, C. Desrosiers, M. Toews, and B. Abdulkarim, Oncotarget. **8**, (2017).
[28] E. A. Jones, S. Deininger, P. C. Hogendoorn, A. M. Deelder, and L. A. McDonnell, J. Proteomics **75**, 16 (2012).
[29] S. Lu, Y. Xia, W. Cai, M. Fulham, and D. D. Feng, Initiative AsDN. Comput. Med. Imaging Graph. **60**, (2017).
[30] D. G. Deschler and T. Day, Otolaryngol Head Neck Surg. (2008).
[31] A. R. Jethwa and S. S. Khariwala, Cancer Metastasis Rev. **36**, 3 (2017).
[32] G. Creff, A. Devillers, A. Depeursinge, X. Palard-Novello, O. Acosta, F. Jegoux, and J. Castelli, JAMA Otolaryngol. Head Neck Surg. (2020).
[33] L. Chen, H. Wang, H. Zeng, Y. Zhang, and X. Ma, Cancer Imaging **20**, 1 (2020).
[34] N. Aide, T. Salomon, C. Blanc-Fournier, J. M. Grellard, C. Levy, and C. Lasnon, EJNMMI Res. **8**, 1 (2018).
[35] Y. Tomori, T. Yamashiro, H. Tomita, M. Tsubakimoto, K. Ishigami, E. Atsumi, and S. Murayama, Eur. J. Radiol. **128**, (2020).
[36] C. Liu, J. Ding, K. Spuhler, Y. Gao, S. M. Serrano, M. Moriarty, S. Jussain, X. He, C. Liang, and C. Huang, J. Magn. Reson. Imaging **49**, 1 (2019).
[37] M. Vallieres, E. Kay-Rivest, L. J. Perrin, X. Liem, C. Furstoss, H. Aerts, N. Khaouam, P. F. Nguyen-Tan, C. S. Wang, K. Sultanem, J. Seuntjens, and I. E. Naqa, Sci. Rep. **7**, 1 (2017).